Biosensors and Bioelectronics 139 (2019) 111328

Contents lists available at ScienceDirect

Biosensors and Bioelectronics

journal homepage: www.elsevier.com/locate/bios

QCM sensing of multivalent interactions between lectins and well-defined glycosylated nanoplatforms

Marta Abellán-Flos[a,1,2], Brian J.J. Timmer[b,1], Samuel Altun[c], Teodor Aastrup[c,*], Stéphane P. Vincent[a,**], Olof Ramström[b,d,e,***]

[a] University of Namur, Département de Chimie, Laboratoire de Chimie Bio-Organique, rue de Bruxelles 61, B-5000, Namur, Belgium
[b] KTH - Royal Institute of Technology, Department of Chemistry, Teknikringen 36, S-100 44, Stockholm, Sweden
[c] Attana AB, Björnnäsvägen 21, SE-114, 19 Stockholm, Sweden
[d] University of Massachusetts Lowell, Department of Chemistry, One University Ave., Lowell, MA, 01854, USA
[e] Linnaeus University, Department of Chemical and Biomedical Sciences, SE-39182, Kalmar, Sweden

ARTICLE INFO

Keywords:
QCM
Carbohydrates
Lectins
Multivalency
Nanoplatforms

ABSTRACT

Quartz crystal microbalance (QCM) methodology has been adopted to unravel important factors contributing to the "cluster glycoside effect" observed in carbohydrate-lectin interactions. Well-defined, glycosylated nanostructures of precise sizes, geometries and functionalization patterns were designed and synthesized, and applied to analysis of the interaction kinetics and thermodynamics with immobilized lectins. The nanostructures were based on Borromean rings, dodecaamine cages, and fullerenes, each of which carrying a defined number of carbohydrate ligands at precise locations. The synthesis of the Borromeates and dodecaamine cages was easily adjustable due to the modular assembly of the structures, resulting in variations in presentation mode. The binding properties of the glycosylated nanoplatforms were evaluated using flow-through QCM technology, as well as hemagglutination inhibition assays, and compared with dodecaglycosylated fullerenes and a monovalent reference. With the QCM setup, the association and dissociation rate constants and the associated equilibrium constants of the interactions could be estimated, and the results used to delineate the multivalency effects of the lectin-nanostructure interactions.

1. Introduction

Cell surface glycans, presented as part of the "glycocalyx" of the cell envelope, play essential roles in the communication between individual cells and their surroundings. Depending on the affinities and selectivities of interactions with different proteins and other carbohydrates, the glycans influence a variety of important processes, such as regulation, modulation, adhesion and infection (Hudak and Bertozzi, 2014; Tarbell and Cancel, 2016; Varki et al., 2009). The carbohydrates also enable the cells to distinguish between native entities and foreign substances, thereby participating in the defense against viruses and bacterial cells. Although the binding selectivities of the various glycan structures are generally high, the efficiencies of these processes also rely on the interaction strengths, where higher binding affinities result in enhancement of the associated processes. Since interactions between monovalent saccharides and their cognate receptors are generally weak, the required affinities can be obtained through the presentation of multiple copies of the participating carbohydrates. This results in multivalent interactions between the glycans and the binding partners, often leading to dramatically enhanced affinities (Badjić et al., 2005; Fasting et al., 2012; Hunter and Anderson, 2009; Mammen et al., 1998). This avidity effect is sometimes referred to as the 'cluster glycoside effect' (Cecioni et al., 2015; Chabre and Roy, 2010; Lee and Lee, 2000; Lundquist and Toone, 2002), effective on both the overall binding and the per mole carbohydrate basis.

To more efficiently control the many processes in which carbohydrates are involved, it is essential to understand this avidity effect. A wide variety of glycosylated architectures has for this reason been

* Corresponding author.
** Corresponding author.
*** Corresponding author. University of Massachusetts Lowell, Department of Chemistry, One University Ave., Lowell, MA, 01854, USA
E-mail addresses: teodor.aastrup@attana.com (T. Aastrup), stephane.vincent@unamur.be (S.P. Vincent), olof_ramstrom@uml.edu (O. Ramström).
[1] These authors contributed equally.
[2] ESPCI Paris, CNRS, PSL University, Molecular, Macromolecular Chemistry and Materials, 10 rue Vauquelin, 75005 Paris, France.

https://doi.org/10.1016/j.bios.2019.111328
Received 26 February 2019; Received in revised form 29 April 2019; Accepted 14 May 2019
Available online 16 May 2019
0956-5663/

developed, *e.g.*, glycodendrimers, glycopolymers, glyconanoparticles and glycoclusters (Bernardi et al., 2013; Chabre and Roy, 2010; Chen et al., 2014; Müller et al., 2016; Ramström and Yan, 2015; Wang et al., 2010; Wittmann and Pieters, 2013). However, for most of these platforms it has been challenging to control the local carbohydrate density and ligand flexibility, and in many cases the asymmetric presentation allows for different modes of interaction. To gain better insight in the important factors contributing to the observed multivalent effects, it is therefore crucial to design well-defined nanoplatforms. In addition, the evaluation of the carbohydrate-presenting entities with equally well-defined binding partners is required to elucidate the different factors determining the binding efficiencies.

These challenges have been addressed in the present study, where we report the synthesis of a range of well-defined glycosylated nanoplatforms and their biological evaluation toward lectins and bacteria using two different methods: real-time quartz crystal microbalance (QCM) methodology (Cheng et al., 2012; Pei et al., 2005), and hemagglutination inhibition assays (HIA) (Durka et al., 2011). The main hypothesis was that precise variations in nanoplatform size, geometry, and residual charge, combined with the carbohydrate structure and presentation, can be used to extract valuable information regarding multivalency effects. By using select lectins with distinct features matching the nanoplatforms, we aimed to draw conclusions regarding the interplay between the different parameters governing the carbohydrate-lectin interactions in these complexes. We thus describe glycosylated nanoplatforms derived from Borromean rings, dodecaamide cages, and fullerenes (Durka et al., 2012; Timmer et al., 2016), for which the binding kinetics and thermodynamics were assessed using QCM against the agglutinins from *Canavalia ensiformis* (ConA) and *Galanthus nivalis* (GNA). We also targeted *Escherichia coli* in order to assess the effect of the glycoclusters directly on the FimH lectin within a cellular context.

2. Materials and methods

2.1. General

All chemicals used for the synthesis of the new compounds were purchased from commercial suppliers (Sigma-Aldrich; NEt_3 and $MgSO_4$ from Alfa Aesar) and used as received. Lectins were purchased from Sigma-Aldrich. All chemicals used for coupling of lectins to the QCM sensor chips were supplied by Attana AB, Sweden. Solid-supported copper catalyst **Cu@A21** was prepared according to a literature procedure (Wu et al., 2014). Hexaalkyne Borromeate **BR·(R^1)$_6$**, dodecaamine cage **C·(R^3)$_{12}$**, azido-functionalized mannoside **1** and all glycosylated nanoplatforms not described below were synthesized according to previously described procedures (Timmer et al., 2016; Abellán Flos et al., 2016; Culshaw et al., 2013; Nierengarten et al., 2010; Tozawa et al., 2009; Chichak et al., 2004, 2005). Anhydrous solvents were obtained by passing them through alumina columns in a Glass Contour solvent dispensing system, or using manual distillation over CaH_2 (CH_2Cl_2, NEt_3). Solvents used during workup, extraction and flash column chromatography were of analytical grade and used as supplied. Flash column chromatography was carried out using Merck silica gel 60 (particle size 0.040–0.063 mm). ATR-IR spectroscopy was performed using a Thermo Scientific Nicolet iS10 spectrophotometer. Mass spectrometry was performed at the Institute of Chemistry at University of Tartu (Estonia). NMR spectra (^{1}H, ^{19}F and ^{13}C) were recorded on either Bruker Avance DMX 500 or Ascend 400 spectrometers. Chemical shifts are reported as δ-values (ppm) relative to tetramethylsilane with (residual) solvent as internal reference.

2.2. Synthesis of glyconanoplatforms

Hexamannoside Borromeate (BR·(R^2)$_6$/BR·6M). Azide functionalized mannoside **1** (7.5 equiv., 75.0 μmol, 22.0 mg) was placed in an oven-dried vial containing a stir bar, **Cu@A21** (25.3 mg, 50 wt% with respect to hexaalkyne **BR·(R^1)$_6$**), and DMSO (500 μL). Hexaalkyne **BR·(R^1)$_6$** (1.0 equiv., 10.0 μmol, 50.6 mg) was added to the solution and the mixture was vortexed, placed under an N_2 atmosphere and stirred at room temperature. After 48 h, the catalyst was removed by filtration over a plug of cotton with the aid of a minimal amount of extra DMSO to minimize product loss. The mixture was concentrated by lyophilization and the product was precipitated by addition of acetone (5 mL). The supernatant was removed and the residue was washed with acetone (5 mL) followed by isopropanol (2 × 5 mL). The residual solids were dried under high vacuum to obtain compound **BR·6M** as a light brown powder (54.5 mg, 7.99 μmol, 80%). ^{1}H NMR (500 MHz, DMSO-d_6, 25 °C) δ = 8.94 (br s, 12H), 8.42–8.09 (m, 24H), 7.42 (br s, 6H), 6.73–6.44 (m, 60H), 5.57 (s, 12 H), 4.84–4.61 (m, 78H), 3.83–3.36 (m, 72H); ^{13}C NMR (126 MHz, DMSO-d_6, 25 °C) δ = 169.7, 167.4, 160.5, 151.3, 149.6, 149.0, 147.9, 140.6, 133.5, 129.5, 125.9, 120.7, 115.9, 111.4, 110.3, 99.9, 73.9, 70.9, 70.2, 69.2, 68.6, 67.0, 65.5, 63.0, 61.2, 60.8, 49.5; ^{19}F NMR (377 MHz, DMSO-d_6, 25 °C) δ 73.5; HRMS (NSI-FTMS, m/z) calc. for $C_{280}H_{264}N_{48}Zn_6O_{76}F_{24}{}^{4+}$ [M-4TFA]$^{4+}$: 1590.8394, found 1590.8444; calc. for $C_{278}H_{264}N_{48}Zn_6O_{74}F_{21}{}^{5+}$ [M-5TFA]$^{5+}$: 1250.0744, found 1250.0773; calc. for $C_{276}H_{264}N_{48}Zn_6O_{72}F_{18}{}^{6+}$ [M-6TFA]$^{6+}$: 1022.8977, found 1022.9002.

Dodecaalkyne Cage (C·(R^4)$_{12}$). 3-(Prop-2-yn-1-yloxy)propanoic acid (18 equiv., 2.7 mmol, 346 mg) was placed in an oven-dried flask containing a stir bar and dissolved in dry toluene (15 mL). Thionyl chloride (54 equiv., 8.1 mmol, 964 mg, 588 μL) was added to the solution and the mixture was heated to 90 °C. After stirring for 6 h, the mixture was cooled down to room temperature and concentrated *in vacuo* to afford compound **2**. In parallel, dodecaamine **C·(R^3)$_{12}$** (122 mg, 0.15 mmol) was suspended in dry CH_2Cl_2 (8 mL), to which NEt_3 (24 equiv., 3.6 mmol, 364 mg, 500 μL) was added. The freshly prepared acid chloride **2** was dissolved in dry CH_2Cl_2 (7 mL) and added dropwise to the mixture containing dodecaamine **C·(R^3)$_{12}$**. The resulting mixture was stirred at r.t. for 16 h, after which it was transferred to a separation funnel containing 5% aqueous NaOH (20 mL) and extracted with CH_2Cl_2 (3 × 30 mL). The combined organic layers were washed with water (10 mL) and dried over $MgSO_4$. The drying agent was removed by filtration and the filtrate was concentrated *in vacuo*. Purification by flash column chromatography using 3.5% MeOH in CH_2Cl_2 to 5% MeOH in CH_2Cl_2 as eluent afforded compound **C·(R^4)$_{12}$** as a clear oily residue (191.2 mg, 0.089 mmol, 60%). ^{1}H NMR (400 MHz, DMSO-d_6, 25 °C) δ = 6.77 (br s, 12H), 4.56–4.11 (m, 48H), 3.70–3.63 (m, 36H), 3.61 (br s, 24H), 2.65 (br s, 24H); ^{13}C NMR (101 MHz, CD_3OD, 25 °C) δ = 173.3, 140.5, 126.6, 80.8, 76.2, 67.3, 59.2, 53.4, 46.5, 34.5; HRMS (NSI-FTMS, m/z) calc. for $C_{120}H_{144}N_{12}O_{24}Na_2{}^{2+}$ [M + 2Na]$^{2+}$:1092.0117, found 1092.0143.

Dodecamannoside Cage (C·(R^5)$_{12}$/CS·12M). Dodecaalkyne **C·(R^4)$_{12}$** (1.0 equiv., 15.8 mg, 7.4 μmol) and azido-functionalized carbohydrate **1** (28 mg, 96 μmol) were placed in a small vial and dissolved in DMSO-d_6 (200 μL). $CuSO_4{\cdot}5H_2O$ (3.0 equiv., 20 μmol, 5 mg) and sodium ascorbate (7.0 equiv., 50 μmol, 10 mg) were added, the vial was capped, and the mixture was stirred at r.t. for 20 h. Addition of MeOH (3 mL) led to precipitation of the product, which was recovered by centrifugation (6000 rpm, 5 min) and removal of the supernatant. The solid was washed by resuspension in MeOH (3 mL), centrifugation (6000 rpm, 5 min) and removal of the supernatant, after which the remainder was dissolved in a minimal amount of water and applied on a column of Sephadex G-25. The product was eluted with water and the fractions containing the product were pooled and treated with Quadrasil® MP (70 mg). After 2 h the solids were removed by filtration and the filtrate was lyophilized to afford the product as a pale yellow sticky oil (7.8 mg, 1.37 μmol, 19%). ^{1}H NMR (500 MHz, DMSO-d_6, 25 °C) δ = 8.03 (br s, 12H), 6.85 (br s, 12H), 4.73–4.49 (m, 84H), 3.80–3.43 (m, 192H), 2.63 (br s, 24H); ^{13}C NMR (126 MHz, DMSO-d_6, 25 °C) δ = 170.6, 143.8, 138.0, 124.2, 99.9, 73.1, 72.0, 70.9, 70.8, 70.2, 70.1, 69.2, 68.6, 66.9, 66.9, 65.9, 65.5, 63.3, 61.2, 61.1, 60.1,

60.0, 49.2, 32.6; HRMS (NSI-FTMS, m/z) calc. for $C_{240}H_{376}N_{48}O_{108}{}^{4+}$ $[M+4H]^{4+}$: 1415.1363, found 1415.1391.

2.3. Hemagglutination inhibition assays

The assays were performed in 96-well round-bottom microtiter plates. Guinea pig erythrocytes (red blood cells, RBCs, Harlan Laboratories) were used as received and diluted to 5% with cold phosphate-buffered saline (PBS, 17 mM K/NaH_2PO_4, 150 mM NaCl). This PBS was used for all further dilutions. Uropathogenic *E. coli* UTI89 cells (clinical isolate engineered for continuous type-1 fimbriation) were grown at 37 °C for 24 h in lysogeny broth (LB, 10 mL). The cells were isolated by centrifugation and washed with cold PBS (3 × 3000 rpm). The hemagglutination unit (HU), *i.e.* the minimum bacteria concentration required to agglutinate RBCs, was first determined by addition of the 5% RBC solution (50 µL) to aliquots (50 µL) of sequential 2-fold dilutions of *E. coli*, and incubation at 4 °C for 1 h. A bacterial concentration of 2 × HU was used for the inhibition assays, performed by adding aliquots (25 µL) of a 2-fold dilution series of the tested compounds (highest concentration: 500 µM) to fixed amounts of bacteria (25 µL) and 5% RBC solution (50 µL). The microtiter plates were then incubated at 4 °C for 1 h, and the hemagglutination titer (HA titer), defined as the lowest concentration resulting in observable hemagglutination, was determined in triplicate for each compound. The obtained results are shown in Fig. S11 and Table S1.

2.4. Quartz crystal microbalance protocols

General Immobilization Protocol. All QCM experiments were performed using a dual-channel Attana Cell 200™ biosensor equipped with an LNB-carboxyl sensor chip in both channels with the flow rate set to 10 µL/min. Depending on the binding affinity, quantity of immobilized ligand and quantity of injected analyte, this instrumentation can detect molecules > 450 Da. Functionalization of the chip surface was performed with 1X HBS-T (10 mM HEPES, 150 mM NaCl and 0.005% Tween) as running buffer. Manual injection of a freshly prepared activation solution containing 1-Ethyl-3-(3-dimethylaminopropyl)carbodiimide (EDC, 0.2 M) with *N*-hydroxysulfosuccinimide (sulfo-NHS, 0.05 M) over both channels for 5 min was followed by manual injection of the lectin over channel 1 only for 5 min. Any unreacted groups were subsequently blocked by treatment of the surfaces with ethanolamine·HCl (1 M) for 5 min on both channels to give lectin functionalized channel 1 and reference channel 2.

General Protocol Binding Experiments. For the binding experiments, the running buffer was changed to a 1X PBS buffer with added Ca^{2+} (0.9 mM $CaCl_2$) and Mg^{2+} (0.49 mM $MgCl_2$) adjusted to pH 7.4 using 1M HCl. The flow rate was adjusted to a rate of 25 µL/min. The samples were prepared by making a two-fold dilution series of the respective compound in the running buffer. For every compound, seven different concentrations were injected with a concentration ranging from 500 to 1.43 µg/mL. The different concentrations of the samples were injected for 84 s in duplicate in random order. All sample injections were followed by a regeneration of the surface with glycine (10 mM glycine, pH 1.5–2.5, 30 s injection). A blank sample was recorded by injection of running buffer at a minimum interval of one per every three sample injections.

General Protocol Kinetic Fitting. The obtained sensorgrams for the functionalized channel 1 were corrected for nonspecific binding by subtraction of the responses obtained from control channel 2. In addition, blank injections were subtracted to correct for background noise. Sensorgrams showing no spikes after correction were generally selected to ensure optimal fitting of the binding models. For fullerene **F·12M** injected over the GNA surface, most sensorgrams showed spikes during the recorded dissociation time, for which reason these were cropped from the data. The data was imported in the Tracedrawer software and the data set was cut after a dissociation time of 350 s. Fitting of a 1:2 binding model using a local B_{max} with no correction for mass transfer effects gave the best fit and provided binding kinetics to differentiate between the monovalent and multivalent binding event.

Interaction Analysis: Concanavalin A. ConA was injected at a concentration of 50 µg/mL in acetate buffer (10 mM, pH 4). A single injection of the lectin at this concentration resulted in a satisfactory functionalization of the sensor chips' surfaces with a response of approximately 50 Hz (cf. Fig. S1). For the regeneration, a 10 mM glycine solution at pH 2.5 proved to be highly efficient to restore the surface treated with the Borromeates (**BR·12M** and **BR·6M**). For the cages **CAr·12M** and **CS·12M**, the surfaces were nearly completely regenerated already after the assigned dissociation time; nevertheless, the regeneration was still performed. Regeneration of the surfaces treated with fullerene **F·12M** was less efficient due to a higher degree of non-specific binding. As all data is corrected for non-specific binding using the unfunctionalized control channel 2, the data obtained for fullerene **F·12M** could still be used to obtain the desired information on binding kinetics. As a result of this non-specific binding on the functionalized chip surface, a lower response was obtained for later injections at the same concentration. The obtained sensorgrams and the fitted kinetic models are shown in Figs. S2–S4.

The sensorgrams obtained for monovalent control **MR·1M** clearly showed saturation binding on the surfaces functionalized with concanavalin A. The low molecular weight of the material resulted in a low frequency shift response of the QCM, for which reason the data was not appropriate for fitting to a binding model in Tracedrawer. Instead the dissociation constant was determined by extracting this value from the saturation isotherm (Fig. S4).

Interaction Analysis: *Galanthus nivalis* Agglutinin. GNA was initially injected at a concentration of 50 µg/mL in acetate buffer (10 mM, pH 4). As unsatisfactory immobilization was obtained after the first injection, due to the similar pH of the immobilization buffer and the pI of the protein, the concentration was increased to 100 µg/mL. Multiple injections of GNA at this concentration provided the desired functionalization of the sensor chips' surfaces with a response of approximately 50 Hz. The obtained sensorgrams for both channel 1 and 2 are provided in Fig. S5.

Similar to concanavalin A, a 10 mM glycine solution was used for regeneration, although a slightly lower pH of 1.5 was proven to be more efficient for the GNA functionalized surface. At this pH, efficient regeneration of the surfaces treated with Borromeates **BR·12M** and **BR·6M**, as well as cage **CAr·12M** was achieved. Cage **CS·12M** and compound **MR·1M** showed no affinity towards the GNA functionalized chip surface under these conditions, but the surface was nevertheless regenerated after injection of these samples. Fullerene **F·12M** again showed a higher degree of nonspecific binding, as apparent from the responses observed for the control channel. The obtained sensorgrams and the fitted kinetic models are shown in Figs. S6–S8.

3. Results and discussion

In a recent study (Timmer et al., 2016), we developed two novel, well-defined carbohydrate nanoplatforms: mannosylated Borromeates and dodecaamide cages (Chichak et al., 2004, 2005; Yates et al., 2007), respectively, using the toolbox provided by constitutional dynamic chemistry (CDC) (Azcune and Odriozola, 2016; Barboiu, 2012; Brachvogel and Delius, 2016; Herrmann, 2014; Hu and Ramström, 2014; Jin et al., 2013; Lehn, 2015; Miller, 2009; Misuraca et al., 2014; Reek and Otto, 2010; Wilson et al., 2014; Zhang and Jin, 2017). Together with mannosylated fullerenes (Cecioni et al., 2011; Durka et al., 2012; Nierengarten et al., 2010; Sánchez-Navarro et al., 2011), these platforms were evaluated with respect to binding behavior, with a main focus placed on the distinctive carbohydrate presentation pattern. These platforms were used as basis in the present study, complemented with additional structures extending the platform range with a higher diversity in ligand densities. The main characteristics of the platforms

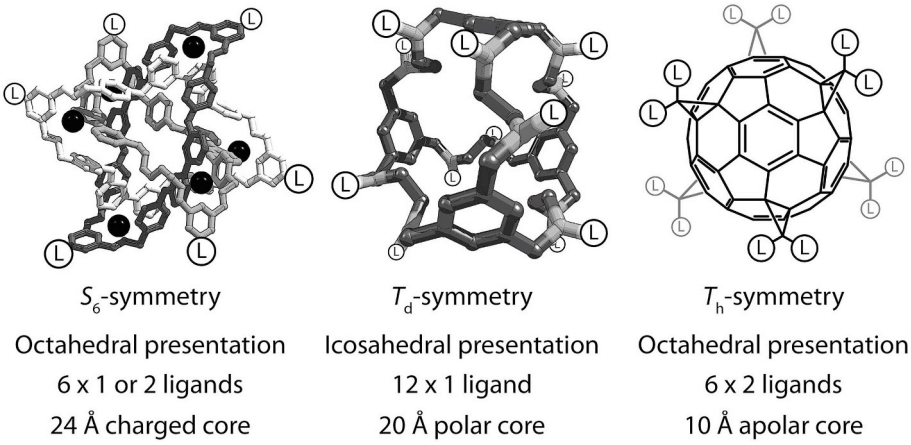

Fig. 1. Characteristics of nanoscaffolds.

are presented in Fig. 1. Each platform type possesses unique properties, which in part overlap with one or both of the others. This enables the distinction of what properties govern specific factors influencing the overall binding to the receptors. The Borromeates and the fullerenes display octahedral presentation of the carbohydrate ligands on their surfaces, but vary in terms of symmetry, charge and size. The dodecaamide cages, on the other hand, display a unique icosahedral ligand presentation mode, have similar size as the Borromeates, and possess an apolar core analogous to the fullerene platform.

Multivalent binding is dependent on both the availability and positioning of the ligands with respect to the receptor. It is therefore desirable to not only study different nanoscaffolds, but also to vary the receptor proteins. Different mannose-specific proteins have in this context been reported to engage in multivalent binding to various extents, of which concanavalin A (ConA) and snowdrop lectin (*Galanthus nivalis* agglutinin, GNA) are shown in Fig. 2 (Branderhorst et al., 2008; Kojori et al., 2016). Both lectins are homotetramers, with GNA (52 kDa) being approximately half the size of ConA (102 kDa), and not being metal-ion dependent (Diederich and Künzer, 1998). The largest difference between the two lectins is observable when comparing their ability to bind mannosides. ConA, having three times less binding sites, binds monovalent saccharides considerably stronger than GNA. This is indicated by a dissociation constant for methyl α-D-mannopyranoside of about 120 μM (Chmielewski et al., 2014; Corbell et al., 2000; Mandal et al., 1994), versus 24 mM observed for GNA (Kaku and Goldstein, 1992). The distance between individual binding sites furthermore

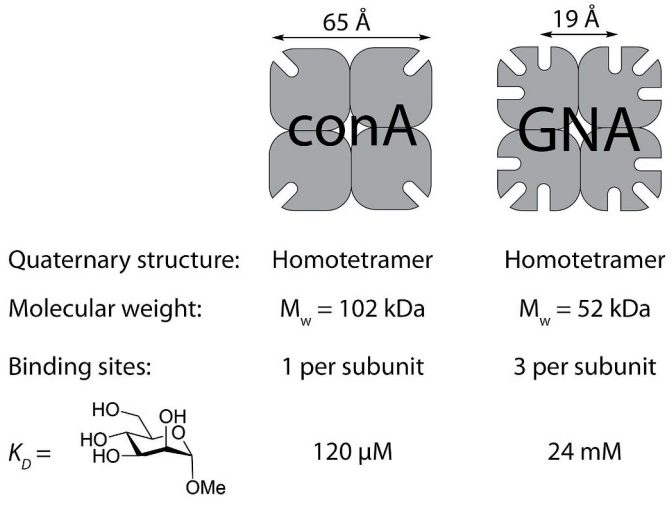

Fig. 2. Structure and characteristics of concanavalin A and snowdrop lectin.

varies between the proteins: 65 Å for ConA and 19 Å for GNA (Diederich and Künzer, 1998), thereby enabling evaluation of potential binding site chelation in the latter case. The isoelectric points of the proteins also differ, where intact ConA displays a pI of ~8 (Bhattacharyya and Brewer, 1990), whereas GNA has a lower pI of < 5, resulting in differences in polyelectrolyte effects with the platforms. For the metalloprotein ConA, isoelectric focusing bands often recorded at lower pH have been attributed to demetalation and aggregation of the apoprotein (Bhattacharyya and Brewer, 1990). Under neutral conditions, GNA is thus expected to have a net negative charge, whereas ConA is expected to have a slight net positive charge. Furthermore, whereas regular binding site chelation with ConA is inaccessible for the studied nanoplatforms, the shorter distance between the binding sites in GNA should allow for the observation of this binding effect.

The different carbohydrate nanoplatforms used in this study are illustrated in Fig. 3. The synthesis of dodecamannosides **BR·12M**, **CAr·12M**, **F·12M** and monovalent reference **MR·1M** was performed as previously reported (Timmer et al., 2016), whereas hexamannosylated Borromeate **BR·6M** was prepared by Cu^{I}-catalyzed azide-alkyne cycloaddition (CuAAC) of an initial hexaalkyne Borromeate with a monovalent mannoside (Scheme S1). All glycocluster structures were assessed by $^{1}H/^{13}C$ NMR, IR, and MS, confirming the full functionalization and resulting high symmetry of the obtained compounds. Hexamannoside **BR·6M** displayed the lowest local carbohydrate density of all multivalent nanoplatforms in this study and also served as control for the affinity differences originating from potential ionic effects by the charged scaffold of the Borromean rings. The additional dodecamannoside cage **CS·12M** was prepared by acylation of the parent, unfunctionalized cage, followed by CuAAC with a monovalent mannoside (Scheme S2). In comparison to **CAr·12M**, the carbohydrates in **CS·12M** are linked using an aliphatic linker. This aliphatic linker was chosen for its reduced rigidity providing the system with a higher degree of conformational freedom. Overall, these carbohydrate nanoplatforms were intended to provide further insight in the importance of statistical and polyelectrolyte effects for multivalent binding.

The obtained carbohydrate nanoplatforms (**BR·12M**, **BR·6M**, **CAr·12M**, **CS·12M**, and **F·12M**), together with monovalent reference **MR·1M**, were evaluated using quartz crystal microbalance instrumentation. This versatile technique offers label-free, real-time analysis of the binding event based on acoustics, providing details with respect to the binding kinetics and thermodynamics (Cheng et al., 2012). The methodology has been used and compared in many studies by us and others (Peiris et al., 2012, 2017; Clausen et al., 2016; Timmer et al., 2016; Li et al., 2013, 2015; Pei et al., 2005), evaluating a wide range of interactions involving small molecules, peptides, proteins, viruses, bacteria, cells, and tissue specimens. Compared to other highly useful techniques, such as SPR and ITC, certain QCM instrumentation

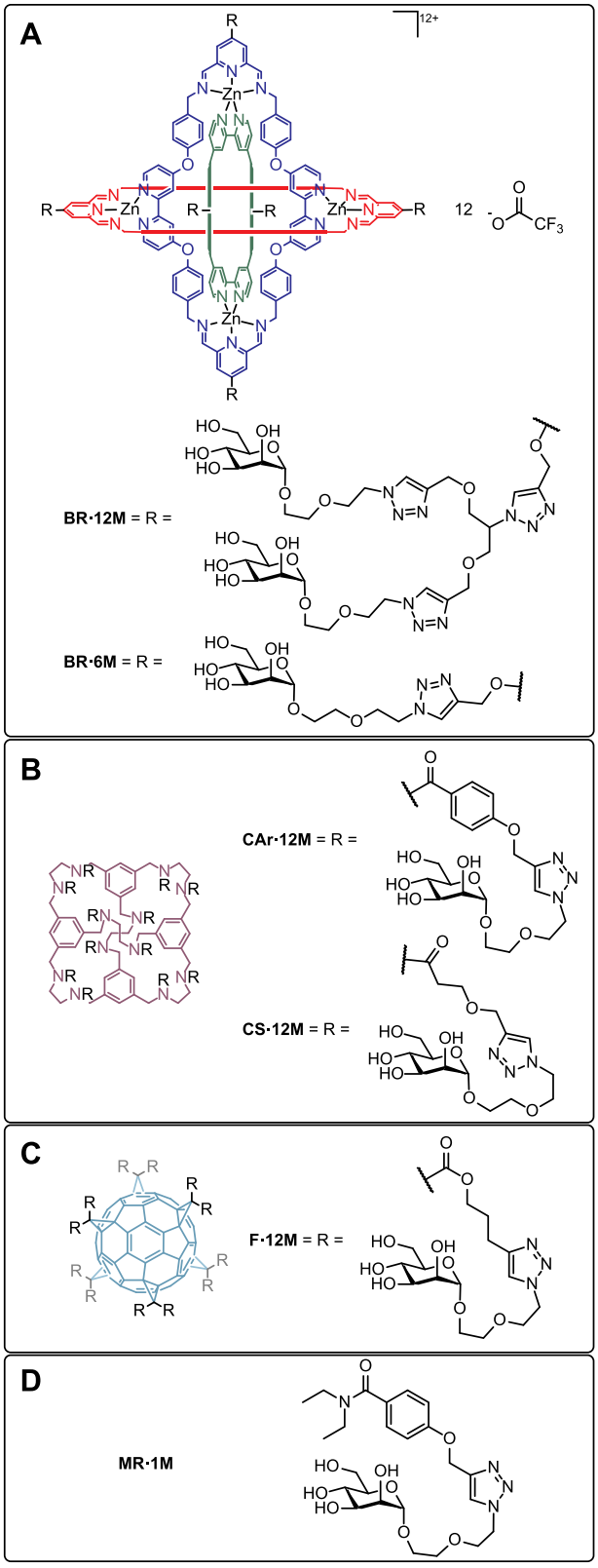

Fig. 3. Structure of (A) glycoborromeate **BR·12M** and **BR·6M**, (B) glycocage **CAr·12M** and **CS·12M**, (C) glycofullerene **F·12M** and (D) monovalent reference **MR·1M**.

can provide a more biologically relevant environment, which results in added value when studying biological interactions.

QCM sensors, carrying a self-assembled monolayer presenting carboxyl end groups, were functionalized with either ConA or GNA through amine coupling. Unreacted groups were subsequently blocked by treatment of the surface with ethanolamine. Conjugation with both ConA (Fig. S1) and GNA (Fig. S5) proved successful, showing frequency shifts (ΔF) of ≈50 Hz for both lectins. The binding events were monitored by injection of eight different concentrations of the respective samples, ranging from 1.43 to 500 μg/mL, over a period of 84 s (35 μL at a 25 μL/min rate), after which the samples were allowed to dissociate from the sensor surface for a minimum of 300 s. Parallel injection of the samples over unfunctionalized QCM sensors allowed for correction for nonspecific binding. After each sample evaluation, both sensor surfaces were regenerated using a 10 mM solution of glycine at pH 2.5 for the ConA experiments and pH 1.5 for the GNA experiments. Regeneration proved highly successful for Borromeates **BR·12M** and **BR·6M** due to instability of the assemblies at this pH, and cages **CAr·12M** and **CS·12M** almost fully dissociated from the sensor surfaces after the assigned dissociation time. Surfaces treated with fullerene **F·12M** could only be partly regenerated even after treatment with glycine, a result of hydrophobic interactions of the apolar fullerene core with the self-assembled monolayer on the sensor surface. As all data is corrected for nonspecific binding and no saturation of the sensor surface was observed, the data obtained for **F·12M** could still be used to obtain the desired information on binding kinetics. The obtained sensorgrams were examined for spikes and other factors that could interfere with proper fitting of the kinetic model. The selected sensorgrams were subjected to kinetic fitting using a 1:2 interaction model to accommodate for both monovalent and multivalent binding. The association rates (k_a), dissociation rates (k_d) and corresponding dissociation constants (K_D) were subsequently extracted from the fitted models.

For the first part of the binding study, ConA-functionalized sensor surfaces were employed. Since the mannose binding sites in this lectin are separated by 65 Å, simultaneous bridging of two binding pockets is not possible for the nanoplatforms in this study, in which the distances between the carbohydrate moieties are shorter. The degree of surface functionalization of the proteins on the QCM chips was furthermore low, thus reducing the possibility for binding of the nanoplatforms between two separate ConA tetramers. Examples of sensorgrams obtained for the glyconanoplatforms are displayed in Fig. 4A (cf. Figs. S2–S4 for all recored and fitted curves). The estimated binding data extracted from the fitted 1:2 binding model are shown in Table 1.

For all studied nanoplatforms, the extracted kinetic data showed one event with higher association and dissociation rates, resulting in weaker affinities, and one event with slower association and dissociation resulting in more stable binding. In our previous study, dissociation constants of 147 nM, 1.21 μM and 1.02 μM were recorded for platforms **BR·12M**, **CAr·12M** and **F·12M**, respectively. When these values were compared with the dissociation constant obtained for monovalent control **MR·1M** (109 μM, Fig. S4), 62-, 8- and 9-fold increases in affinity per carbohydrate (relative potencies, *RPs*) were obtained for these platforms (cf. Table S1). Overall, the higher distribution of the ligands in cage **CAr·12M** results in a lower local concentration of carbohydrates at the binding site with this platform. This is suggested to weaken the interactions between the platform and the protein, resulting in the observed higher dissociation rate. In comparison, both octahedrally substituted platforms **BR·12M** and **F·12M** have a less distributed presentation of the carbohydrates at the scaffold periphery, however still displaying a clear difference in binding affinity to ConA. This indicates that either the forced higher spatial distribution by the cyclopropane functionalization in fullerene **F·12M**, combined with the size difference of the core structures, affects the binding properties, or that secondary interactions or polyelectrolyte effects contribute to the observed increase in affinity.

To support these observations, the modified nanoplatforms **BR·6M** and **CS·12M** were subjected to the same binding experiments. From the kinetic data obtained for hexamannoside **BR·6M**, it can be seen that the overall dissociation constant (152 nM) is comparable to the value obtained for dodecamannoside **BR·12M** (147 nM). Since nanoplatform

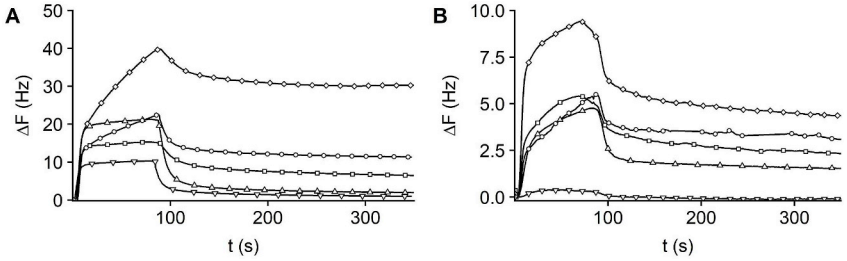

Fig. 4. Example sensorgrams after subtraction of control channel signal for binding of **BR·12M** (◇), **BR·6M** (□), **CAr·12M** (△), **CS·12M** (▽) and **F·12M** (○) to sensor surfaces functionalized with ConA (A) and GNA (B).

BR·6M presents six mannose residues, a 120-fold increase in affinity per carbohydrate could be obtained in comparison to monovalent control **MR·1M**. However, even though similar overall dissociation constants were estimated for both glycoborromeates, the obtained sensorgrams indicate a clear difference in binding behavior. Platform **BR·6M** showed a higher dissociation rate than Borromeate **BR·12M** and resulted in equilibrium formation. This result was expected owing to the lower degree of carbohydrate functionalization in this platform. The comparable dissociation constants of the platforms also originate from the increase in association rate of the hexavalent Borromeate, which is likely a result of the slightly different linker characteristics of this platform compared to Borromeate **BR·12M**. Owing to the relatively short linkers between the charged platform and the carbohydrates of platform **BR·6M**, the increased association rate indicates that a polyelectrolyte effect is not pronounced in this binding event. A higher degree of electrostatic repulsion would otherwise have been expected due to decreased distances between the charged platform and the carbohydrate.

For the cage with the aliphatic linker (**CS·12M**), rapid dissociation from the surfaces was observed in analogy to cage **CAr·12M** carrying an aromatic linker. Due to the increase in conformational freedom of the linked carbohydrates, it is less probable that subsite interactions occur after initial binding. As expected, the dissociation constant increased from 1.21 μM for cage **CAr·12M** to 3.68 μM for **CS·12M** as a result of the decreased association rate for the multivalent binding event. Overall, this reduces the enhanced affinity per carbohydrate to 2.5-fold for cage **CS·12M** in comparison to monovalent reference **MR·1M**.

To investigate if polyelectrolyte and statistical effects are important for binding of the glycosylated nanoplatforms to other lectins, similar binding experiments were performed with GNA-functionalized surfaces. As mentioned earlier, the shorter distance (19 Å) between the mannose binding sites in GNA can allow for bridging of two binding pockets by different mannose residues on the investigated glyconanoplatforms. Since all studied nanoplatforms present carbohydrates within this distance, it was expected that the spatial presentation of the carbohydrates would be of less importance. Examples of the resulting sensorgrams obtained for every glyconanoplatform are shown in Fig. 4B (cf. Figs. S6–S8 for all measured and fitted curves). The estimated rate and binding constants after fitting of the data to a 1:2 binding model are shown in Table 2.

The results indicate that similar dissociation behavior was observed for **BR·12M**, **CAr·12M** and **F·12M** when detaching from the GNA functionalized QCM sensor. This is also reflected in the extracted kinetic data from the fitted sensorgrams, showing similar dissociation rates for both the monovalent and multivalent events. As expected, a main contribution to the observed multivalent effect for GNA likely originates from the ability to bridge separate binding sites. However, the estimated dissociation constant for dodecamannoside **BR·12M** (77 nM) was considerably lower than the values observed for cage **CAr·12M** (1.12 μM) and fullerene **F·12M** (1.49 μM), respectively. This indicates that a large contribution to the affinity enhancement of Borromeate **BR·12M** is likely to originate from the polyelectrolyte effect, providing this positively charged platform with a higher association rate to the predominantly negatively charged GNA-functionalized surface. As the monovalent reference **MR·1M** did not show any measurable affinity to the GNA functionalized surface, the enhancement in affinity per carbohydrate could not be accurately determined using the QCM method. However, from the previously observed dissociation constant for methyl α-D-mannopyranoside (24 mM) (Kaku and Goldstein, 1992), relative potencies of 1300–26000 per carbohydrate unit can be deduced.

The binding features of hexavalent Borromeate **BR·6M** and dodecavalent cage **CS·12M** against GNA were furthermore evaluated. Interestingly, cage **CS·12M** showed no quantifiable affinity to the surfaces, suggesting that an increase in rotational freedom due to the aliphatic linkers again led to a decrease in affinity. For the hexavalent Borromeate **BR·6M**, a slight decrease in affinity (K_{D2} = 206 nM) was observed in comparison to dodecavalent Borromeate **BR·12M** (K_{D2} = 76.6 nM). Since the estimated dissociation rates were similar for both nanoplatforms, the difference in dissociation constant is mainly due to the decrease in the association rate for hexamannoside **BR·6M**, a result likely due to the reduced availability of mannosides of this platform. Overall, the affinity observed per carbohydrate unit was enhanced 19000-fold for Borromeate **BR·6M**, a value of the same order of magnitude as that observed for dodecamannoside **BR·12M**.

The ability of the glycoclusters to directly bind bacterial adhesins

Table 1
Association rates, dissociation rates and dissociation constants obtained for binding of mannosylated structures to a ConA-functionalized QCM chip.

Glycosylated scaffold	k_{a1} ($M^{-1}s^{-1}$)	k_{d1} (s^{-1})	K_{D1} (M)	k_{a2} ($M^{-1}s^{-1}$)	k_{d2} (s^{-1})	K_{D2} (M)
BR·12M	4.72×10^{4} $\pm 1.34 \times 10^{3}$	5.59×10^{-2} $\pm 1.19 \times 10^{-5}$	1.19×10^{-6} $\pm 3.38 \times 10^{-8}$	1.31×10^{3} $\pm 3.92 \times 10^{2}$	1.93×10^{-4} $\pm 3.98 \times 10^{-5}$	**1.47×10^{-7} $\pm 8.17 \times 10^{-8}$**
CAr·12M	9.52×10^{3} $\pm 6.82 \times 10^{2}$	1.01×10^{-1} $\pm 6.34 \times 10^{-5}$	1.06×10^{-5} $\pm 8.22 \times 10^{-8}$	1.67×10^{3} $\pm 3.19 \times 10^{3}$	2.02×10^{-3} $\pm 5.23 \times 10^{-5}$	**1.21×10^{-6} $\pm 8.86 \times 10^{-7}$**
F·12M	2.73×10^{4} $\pm 1.35 \times 10^{3}$	8.70×10^{-2} $\pm 7.75 \times 10^{-6}$	3.18×10^{-6} $\pm 1.57 \times 10^{-7}$	6.50×10^{2} $\pm 3.26 \times 10^{2}$	6.63×10^{-4} $\pm 8.28 \times 10^{-6}$	**1.02×10^{-6} $\pm 7.00 \times 10^{-7}$**
BR·6M	1.15×10^{4} $\pm 4.35 \times 10^{1}$	5.49×10^{-2} $\pm 2.50 \times 10^{-4}$	4.76×10^{-6} $\pm 3.96 \times 10^{-8}$	6.87×10^{3} $\pm 7.35 \times 10^{2}$	1.04×10^{-3} $\pm 3.18 \times 10^{-5}$	**1.52×10^{-7} $\pm 2.11 \times 10^{-8}$**
CS·12M	6.86×10^{3} $\pm 4.12 \times 10^{1}$	7.83×10^{-2} $\pm 3.54 \times 10^{-4}$	1.14×10^{-5} $\pm 1.20 \times 10^{-7}$	6.93×10^{2} $\pm 8.47 \times 10^{1}$	2.55×10^{-3} $\pm 1.12 \times 10^{-4}$	**3.68×10^{-6} $\pm 6.21 \times 10^{-7}$**
MR·1M[a]	–	–	–	–	–	**1.09×10^{-4} $\pm 0.19 \times 10^{-4}$**

[a] Determined from saturation binding due to low response observed in the sensorgrams.

Table 2
Association rates, dissociation rates and dissociation constants obtained for binding of the different samples to a GNA functionalized QCM chip.

Glycosylated scaffold	k_{a1} ($M^{-1}s^{-1}$)	k_{d1} (s^{-1})	K_{D1} (M)	k_{a2} ($M^{-1}s^{-1}$)	k_{d2} (s^{-1})	K_{D2} (M)
BR·12M	$2.69 \times 10^4 \pm 2.16 \times 10^3$	$1.13 \times 10^{-1} \pm 7.74 \times 10^{-6}$	$4.18 \times 10^{-6} \pm 3.39 \times 10^{-7}$	$1.06 \times 10^4 \pm 1.52 \times 10^3$	$8.14 \times 10^{-4} \pm 3.20 \times 10^{-6}$	$\mathbf{7.66 \times 10^{-8} \pm 1.15 \times 10^{-8}}$
CAr·12M	$1.93 \times 10^3 \pm 4.11 \times 10^2$	$1.20 \times 10^{-1} \pm 1.86 \times 10^{-6}$	$6.12 \times 10^{-5} \pm 1.39 \times 10^{-5}$	$5.96 \times 10^2 \pm 2.40 \times 10^2$	$6.68 \times 10^{-4} \pm 2.53 \times 10^{-6}$	$\mathbf{1.12 \times 10^{-6} \pm 5.44 \times 10^{-7}}$
F·12M	$2.14 \times 10^4 \pm 6.37 \times 10^3$	$1.52 \times 10^{-1} \pm 3.71 \times 10^{-5}$	$7.08 \times 10^{-5} \pm 2.31 \times 10^{-6}$	$4.70 \times 10^2 \pm 7.24 \times 10^1$	$7.00 \times 10^{-4} \pm 1.81 \times 10^{-6}$	$\mathbf{1.49 \times 10^{-6} \pm 2.39 \times 10^{-7}}$
BR·6M	$1.38 \times 10^4 \pm 5.19 \times 10^3$	$8.62 \times 10^{-2} \pm 1.81 \times 10^{-5}$	$6.23 \times 10^{-6} \pm 2.72 \times 10^{-6}$	$4.02 \times 10^3 \pm 9.40 \times 10^2$	$8.30 \times 10^{-4} \pm 1.91 \times 10^{-6}$	$\mathbf{2.06 \times 10^{-7} \pm 5.16 \times 10^{-8}}$
CS·12M[a]	–	–	–	–	–	–
MR·1M[a]	–	–	–	–	–	–

[a] Kinetic data not determined due to too weak binding to sensor surface.

was finally evaluated. In these studies, the α-D-mannoside-specific FimH lectin expressed on type 1 pili of *E. coli* was targeted (Krogfelt et al., 1990). This lectin enables the adhesion of uropathogenic *E. coli* to the bladder epithelium, which is a critical factor in development of urinary tract infections (Hartmann and Lindhorst, 2011). Initially, attempts were made to evaluate the binding of the glyconanoplatforms to bacteria immobilized on QCM chips. For this, the two *E. coli* strains ORN178 (Pil^+, *fimH*+ (Russell and Orndorff, 1992), binds α-D-mannosides) and ORN208 (Pil^+, *fimH*-mutant (*fimH304::kan*) (Harris et al., 2001), does not bind α-D-mannosides) were immobilized on the two different channels. Unfortunately, the immobilized quantity of bacteria was either too low, or the binding of the studied nanoplatforms to the bacteria was too weak to produce quantifiable responses. As expected, Borromeate **BR·12M** showed high nonspecific affinity to both surfaces due to charge-based interactions of the positively charged platform with the negatively charged surface of the bacteria (Fig. S10), again indicating the importance of matching polyelectrolyte effects in observed binding effects. For these reasons, hemagglutination inhibition assays were instead adopted, using Guinea pig erythrocytes and uropathogenic *E. coli* strain UTI89 (Pil^+, $fimH^+$, binds α-D-mannosides) (Chen et al., 2006; Durka et al., 2011). Platforms **BR·12M**, **CAr·12M** and **F·12M** were compared to the monovalent probe **MR·1M**, and CuI was furthermore tested as a control to exclude effects from potential traces of Cu ions. The results showed that all three platforms displayed moderate inhibitory enhancements ($\beta = 16–32$), of which fullerene **F·12M** had slightly lower hemagglutination titer (× 2) and thereby higher relative potency (× 2) than Borromeate **BR·12M** and cage **CAr·12M** (cf. Fig. S11,Table S1). These results could be expected, since FimH is a monomeric adhesin that is more unlikely to produce large multivalent effects.

4. Conclusions

In summary, we have shown that the toolbox provided by constitutional dynamic chemistry and fullerene chemistry can give access to symmetric scaffolds for the synthesis of well-defined, precisely mannosylated nanoplatforms of various symmetry, charge and size. Introduction of small alterations to the glycosylation procedure furthermore enabled efficient access to customized structures and led to a series of glyconanoplatforms that could be used to unravel important factors underlying observed multivalent binding effects. Using quartz crystal microbalance technology, the affinities of these nanoplatforms for surface-immobilized mannose-binding lectins, possessing different binding features, were evaluated and compared with monovalent references. The results showed that the effects of an optimal carbohydrate distribution pattern, leading to better adapted local densities, appeared dominant in the absence of the possibility to bridge different binding sites or matching polyelectrolyte effects. When such effects were feasible, as recorded with the smaller *Galanthus nivalis* agglutinin, the spatial distribution of carbohydrates showed limited influence and similar dissociation rates were observed for all platforms. Overall, this study underscores that the observed "cluster glycoside effect" is not solely dependent on the type and quantity of carbohydrate units, but that the exact distribution pattern, the flexibility of the structures, the size and symmetry of the scaffold, as well as polyelectrolyte effects provide important contributions to the affinity.

Acknowledgements

This project received funding from the European Union's Seventh Framework Programme for research, technological development and demonstration under grant agreement no 289033.

Appendix A. Supplementary data

Supplementary data to this article can be found online at https://doi.org/10.1016/j.bios.2019.111328.

References

Abellán Flos, M., García Moreno, M.I., Ortiz Mellet, C., García Fernández, J.M., Nierengarten, J.-F., Vincent, S.P., 2016. Potent glycosidase inhibition with heterovalent fullerenes: unveiling the binding modes triggering multivalent inhibition. Chem. Eur J. 22, 11450–11460. https://doi.org/10.1002/chem.201601673.

Azcune, I., Odriozola, I., 2016. Aromatic disulfide crosslinks in polymer systems: self-healing, reprocessability, recyclability and more. Eur. Polym. J. 84, 147–160. https://doi.org/10.1016/j.eurpolymj.2016.09.023.

Badjić, J.D., Nelson, A., Cantrill, S.J., Turnbull, W.B., Stoddart, J.F., 2005. Multivalency and cooperativity in supramolecular chemistry. Acc. Chem. Res. 38, 723–732. https://doi.org/10.1021/ar040223k.

Barboiu, M., 2012. Constitutional Dynamic Chemistry. Springer Verlag, Berlin Heidelberg.

Bernardi, A., Jiménez-Barbero, J., Casnati, A., De Castro, C., Darbre, T., Fieschi, F., Finne, J., Funken, H., Jaeger, K.-E., Lahmann, M., Lindhorst, T.K., Marradi, M., Messner, P., Molinaro, A., Murphy, P.V., Nativi, C., Oscarson, S., Penadés, S., Peri, F., Pieters, R.J., Renaudet, O., Reymond, J.-L., Richichi, B., Rojo, J., Sansone, F., Schäffer, C., Turnbull, W.B., Velasco-Torrijos, T., Vidal, S., Vincent, S., Wennekes, T., Zuilhof, H., Imberty, A., 2013. Multivalent glycoconjugates as anti-pathogenic agents. Chem. Soc. Rev. 42, 4709–4727. https://doi.org/10.1039/c2cs35408j.

Bhattacharyya, L., Brewer, C.F., 1990. Isoelectric focusing studies of concanavalin A and the lentil lectin. J. Chromatogr. 502, 131–142. https://doi.org/10.1016/S0021-9673(01)89570-4.

Brachvogel, R.-C., Delius, M. von, 2016. The dynamic covalent chemistry of esters, acetals and orthoesters. Eur. J. Org. Chem. 2016, 3662–3670. https://doi.org/10.1002/ejoc.201600388.

Branderhorst, H.M., Ruijtenbeek, R., Liskamp, R.M.J., Pieters, R.J., 2008. Multivalent carbohydrate recognition on a glycodendrimer-functionalized flow-through chip. Chembiochem 9, 1836–1844. https://doi.org/10.1002/cbic.200800195.

Cecioni, S., Imberty, A., Vidal, S., 2015. Glycomimetics versus multivalent glycoconjugates for the design of high affinity lectin ligands. Chem. Rev. 115, 525–561. https://doi.org/10.1021/cr500303t.

Cecioni, S., Oerthel, V., Iehl, J., Holler, M., Goyard, D., Praly, J.P., Imberty, A., Nierengarten, J.F., Vidal, S., 2011. Synthesis of dodecavalent fullerene-based glycoclusters and evaluation of their binding properties towards a bacterial lectin. Chem. Eur J. 17, 3252–3261. https://doi.org/10.1002/chem.201003258.

Chabre, Y.M., Roy, R., 2010. Design and creativity in synthesis of multivalent neoglycoconjugates. Adv. Carbohydr. Chem. Biochem. 63, 165–393. https://doi.org/10.1016/S0065-2318(10)63006-5.

Chen, S.L., Hung, C.-S., Xu, J., Reigstad, C.S., Magrini, V., Sabo, A., Blasiar, D., Bieri, T., Meyer, R.R., Ozersky, P., Armstrong, J.R., Fulton, R.S., Latreille, J.P., Spieth, J., Hooton, T.M., Mardis, E.R., Hultgren, S.J., Gordon, J.I., 2006. Identification of genes

subject to positive selection in uropathogenic strains of escherichia coli: a comparative genomics approach. In: Proc. Natl. Acad. Sci. U.S.A., vol. 103. pp. 5977–5982. https://doi.org/10.1073/pnas.0600938103.
Chen, X., Ramström, O., Yan, M., 2014. Glyconanomaterials: emerging applications in biomedical research. Nano Res 7, 1381–1403. https://doi.org/10.1007/s12274-014-0507-y.
Cheng, H., Byrska-Bishop, M., Zhang, C.T., Kastrup, C.J., Hwang, N.S., Tai, A.K., Lee, W.W., Xu, X., Nahrendorf, M., Langer, R., Anderson, D.G., 2012. Stem cell membrane engineering for cell rolling using peptide conjugation and tuning of cell–selectin interaction kinetics. Biomaterials 33, 5004–5012. https://doi.org/10.1016/j.biomaterials.2012.03.065.
Chichak, K.S., Cantrill, S.J., Pease, A.R., Chiu, S.-H., Cave, G.W.V., Atwood, J.L., Stoddart, J.F., 2004. Molecular borromean rings. Science 304, 1308–1312. https://doi.org/10.1126/science.1096914.
Chichak, K.S., Peters, A.J., Cantrill, S.J., Stoddart, J.F., 2005. Nanoscale Borromeates. J. Org. Chem. 70, 7956–7962. https://doi.org/10.1021/jo050969b.
Chmielewski, M.J., Buhler, E., Candau, J., Lehn, J.-M., 2014. Multivalency by self-assembly: binding of concanavalin a to metallosupramolecular architectures decorated with multiple carbohydrate groups. Chem. Eur J. 20, 6960–6977. https://doi.org/10.1002/chem.201304511.
Clausen, T.M., Pereira, M.A., Oo, H.Z., Resende, M., Gustavson, T., Mao, Y., Sugiura, N., Liew, J., Fazli, L., Theander, T.G., Daugaard, M., Salanti, A., 2016. Real-time and label free determination of ligand binding-kinetics to primary cancer tissue specimensmathsemicolon a novel tool for the assessment of biomarker targeting. Sens. Bio-Sens. Res. 9, 23–30. https://doi.org/10.1016/j.sbsr.2016.05.003.
Corbell, J.B., Lundquist, J.J., Toone, E.J., 2000. A comparison of biological and calorimetric analyses of multivalent glycodendrimer ligands for concanavalin a. Tetrahedron: Asymmetry 11, 95–111. https://doi.org/10.1016/s0957-4166(99)00589-3.
Culshaw, J.L., Cheng, G., Schmidtmann, M., Hasell, T., Liu, M., Adams, D.J., Cooper, A.I., 2013. Dodecaamide cages: organic 12-arm building blocks for supramolecular chemistry. J. Am. Chem. Soc. 135, 10007–10010. https://doi.org/10.1021/ja403987j.
Diederich, F., Künzer, H. (Eds.), 1998. Recent Trends in Molecular Recognition. Springer. https://doi.org/10.1007/978-3-662-03574-0.
Durka, M., Buffet, K., Iehl, J., Holler, M., Nierengarten, J.-F., Taganna, J., Bouckaert, J., Vincent, S.P., 2011. The functional valency of dodecamannosylated fullerenes with Escherichia coli FimH–towards novel bacterial antiadhesives. Chem. Commun. (Camb). 47, 1321–1323. https://doi.org/10.1039/c0cc04468g.
Durka, M., Buffet, K., Iehl, J., Holler, M., Nierengarten, J.F., Vincent, S.P., 2012. The inhibition of liposaccharide heptosyltransferase WaaC with multivalent glycosylated fullerenes: a new mode of glycosyltransferase inhibition. Chem. Eur J. 18, 641–651. https://doi.org/10.1002/chem.201102052.
Fasting, C., Schalley, C.A., Weber, M., Seitz, O., Hecht, S., Koksch, B., Dernedde, J., Graf, C., Knapp, E.-W., Haag, R., 2012. Multivalency as a chemical organization and action principle. Angew. Chem. Int. Ed. 51, 10472–10498. https://doi.org/10.1002/anie.201201114.
Harris, S.L., Spears, P.A., Havell, E.A., Hamrick, T.S., Horton, J.R., Orndorff, P.E., 2001. Characterization of Escherichia coli type 1 pilus mutants with altered binding specificities. J. Bacteriol. 183, 4099–4102. https://doi.org/10.1128/JB.183.13.4099-4102.2001.
Hartmann, M., Lindhorst, T.K., 2011. The bacterial lectin FimH, a target for drug discovery - carbohydrate inhibitors of type 1 fimbriae-mediated bacterial adhesion. Eur. J. Org. Chem. 2011, 3583–3609. https://doi.org/10.1002/ejoc.201100407.
Herrmann, A., 2014. Dynamic combinatorial/covalent chemistry: a tool to read, generate and modulate the bioactivity of compounds and compound mixtures. Chem. Soc. Rev. 43, 1899–1933. https://doi.org/10.1039/c3cs60336a.
Hu, L., Ramström, O., 2014. Silver-catalyzed dynamic systemic resolution of α-iminonitriles in a 1,3-dipolar cycloaddition process. Chem. Commun. 50, 3792–3794. https://doi.org/10.1039/c4cc00944d.
Hudak, J.E., Bertozzi, C.R., 2014. Glycotherapy: new advances inspire a reemergence of glycans in medicine. Chem. Biol. 21, 16–37. https://doi.org/10.1016/j.chembiol.2013.09.010.
Hunter, C.A., Anderson, H.L., 2009. What is cooperativity? Angew. Chem. Int. Ed. 48, 7488–7499. https://doi.org/10.1002/anie.200902490.
Jin, Y., Yu, C., Denman, R.J., Zhang, W., 2013. Recent advances in dynamic covalent chemistry. Chem. Soc. Rev. 42, 6634–6654. https://doi.org/10.1039/c3cs60044k.
Kaku, H., Goldstein, I.J., 1992. Interaction of linear manno-oligosaccharides with three mannose-specific bulb lectins. Comparison with mannose/glucose-binding lectins. Carbohydr. Res. 229, 337–346. https://doi.org/10.1016/s0008-6215(00)90579-2.
Kojori, H.S., Ji, Y., Paik, Y., Braunschweig, A.B., Kim, S.J., 2016. Monitoring interfacial lectin binding with nanomolar sensitivity using a plasmon field effect transistor. Nanoscale 8, 17357–17364. https://doi.org/10.1039/c6nr05544c.
Krogfelt, K.A., Bergmans, H., Klemm, P., 1990. Direct evidence that the FimH protein is the mannose-specific adhesin of Escherichia coli type 1 fimbriae. Infect. Immun. 58, 1995–1998.
Lee, R.T., Lee, Y.C., 2000. Affinity enhancement by multivalent lectin–carbohydrate interaction. Glycoconj. J. 17, 543–551. https://doi.org/10.1023/a:1011070425430.
Lehn, J.-M., 2015. Perspectives in chemistry-aspects of adaptive chemistry and materials. Angew. Chem. Int. Ed. 54, 3276–3289. https://doi.org/10.1002/anie.201409399.
Li, X., Pei, Y., Zhang, R., Shuai, Q., Wang, F., Aastrup, T., Pei, Z., 2013. A suspension-cell biosensor for real-time determination of binding kinetics of protein–carbohydrate interactions on cancer cell surfaces. Chem. Commun. 49 (9908). https://doi.org/10.1039/c3cc45006f.
Li, X., Song, S., Shuai, Q., Pei, Y., Aastrup, T., Pei, Y., Pei, Z., 2015. Real-time and label-free analysis of binding thermodynamics of carbohydrate-protein interactions on unfixed cancer cell surfaces using a QCM biosensor. Sci. Rep. 5. https://doi.org/10.1038/srep14066.
Lundquist, J.J., Toone, E.J., 2002. The cluster glycoside effect. Chem. Rev. 102, 555–578. https://doi.org/10.1021/cr000418f.
Mammen, M., Choi, S.K., Whitesides, G.M., 1998. Polyvalent interactions in biological systems: implications for design and use of multivalent ligands and inhibitors. Angew. Chem. Int. Ed. 37, 2755–2794. https://doi.org/10.1002/(SICI)1521-3773(19981102)37:20<2754::AID-ANIE2754>3.0.CO;2-3.
Mandal, D.K., Kishore, N., Brewer, C.F., 1994. Thermodynamics of lectin-carbohydrate interactions. Titration microcalorimetry measurements of the binding of N-linked carbohydrates and ovalbumin to concanavalin A. Biochemistry 33, 1149–1156. http://doi.org/10.1021/bi00171a014.
Miller, B.L., 2009. Dynamic combinatorial chemistry. In: Drug Discovery, Bioorganic Chemistry, and Materials Science. John Wiley & Sons, Inc., Hoboken, NJ.
Misuraca, M.C., Moulin, E., Ruff, Y., Giuseppone, N., 2014. Experimental and theoretical methods for the analyses of dynamic combinatorial libraries. New J. Chem. 38, 3336–3349. https://doi.org/10.1039/C4NJ00304G.
Müller, C., Despras, G., Lindhorst, T.K., 2016. Organizing multivalency in carbohydrate recognition. Chem. Soc. Rev. 45, 3275–3302. https://doi.org/10.1039/c6cs00165c.
Nierengarten, J.-F., Iehl, J., Oerthel, V., Holler, M., Illescas, B.M., Muñoz, A., Martín, N., Rojo, J., Sánchez-Navarro, M., Cecioni, S., Vidal, S., Buffet, K., Durka, M., Vincent, S.P., 2010. Fullerene sugar balls. Chem. Commun. 46, 3860–3862. https://doi.org/10.1039/c0cc00034e.
Pei, Z., Anderson, H., Aastrup, T., Ramström, O., 2005. Study of real-time lectin-carbohydrate interactions on the surface of a quartz crystal microbalance. Biosens. Bioelectron. 21, 60–66. https://doi.org/10.1016/j.bios.2004.10.006.
Peiris, D., Markiv, A., Curley, G.P., Dwek, M.V., 2012. A novel approach to determining the affinity of protein-carbohydrate interactions employing adherent cancer cells grown on a biosensor surface. Biosens. Bioelectron. 35, 160–166. https://doi.org/10.1016/j.bios.2012.02.037.
Peiris, D., Spector, A.F., Lomax-Browne, H., Azimi, T., Ramesh, B., Loizidou, M., Welch, H., Dwek, M.V., 2017. Cellular glycosylation affects Herceptin binding and sensitivity of breast cancer cells to doxorubicin and growth factors. Sci. Rep. 7. https://doi.org/10.1038/srep43006.
Ramström, O., Yan, M., 2015. Glyconanomaterials for combating bacterial infections. Chem. Eur J. 21, 16310–16317. https://doi.org/10.1002/chem.201502842.
Reek, J.N.H., Otto, S., 2010. Dynamic Combinatorial Chemistry. Wiley-VCH Verlag GmbH & Co. KGaA, Weinheim, Germany.
Russell, P.W., Orndorff, P.E., 1992. Lesions in two escherichia coli type 1 pilus genes alter pilus number and length without affecting receptor binding. J. Bacteriol. 174, 5923–5935. https://doi.org/10.1128/jb.174.18.5923-5935.1992.
Sánchez-Navarro, M., Muñoz, A., Illescas, B.M., Rojo, J., Martín, N., 2011. [60]Fullerene as multivalent scaffold: efficient molecular recognition of globular glycofullerenes by concanavalin A. Chem. Eur J. 17, 766–769. https://doi.org/10.1002/chem.201002816.
Tarbell, J.M., Cancel, L.M., 2016. The glycocalyx and its significance in human medicine. J. Intern. Med. 280, 97–113. https://doi.org/10.1111/joim.12465.
Timmer, B.J.J., Abellán Flos, M., Jørgensen, L.M., Proverbio, D., Altun, S., Ramström, O., Aastrup, T., Vincent, S.P., 2016. Spatially well-defined carbohydrate nanoplatforms: synthesis, characterization and lectin interaction study. Chem. Commun. 52, 12326–12329. https://doi.org/10.1039/C6CC06737A.
Tozawa, T., Jones, J.T. a, Swamy, S.I., Jiang, S., Adams, D.J., Shakespeare, S., Clowes, R., Bradshaw, D., Hasell, T., Chong, S.Y., Tang, C., Thompson, S., Parker, J., Trewin, A., Bacsa, J., Slawin, A.M.Z., Steiner, A., Cooper, A.I., 2009. Porous organic cages. Nat. Mater., Nat. Mater. 8, 973–978. https://doi.org/10.1038/nmat2545.
Varki, A., Cummings, R.D., Esko, J.D., Freeze, H.H., Stanley, P., Bertozzi, C.R., Hart, G.W., Etzler, M.E., 2009. Essentials of Glycobiology. Cold Spring Harbor Laboratory Press, New York.
Wang, X., Ramström, O., Yan, M., 2010. Glyconanomaterials: synthesis, characterization, and ligand presentation. Adv. Mater. 22, 1946–1953. https://doi.org/10.1002/adma.200903908.
Wilson, A., Gasparini, G., Matile, S., 2014. Functional systems with orthogonal dynamic covalent bonds. Chem. Soc. Rev. 43, 1948–1962. https://doi.org/10.1039/c3cs60342c.
Wittmann, V., Pieters, R.J., 2013. Bridging lectin binding sites by multivalent carbohydrates. Chem. Soc. Rev. 42, 4492. https://doi.org/10.1039/c3cs60089k.
Wu, H., Li, H., Kwok, R.T.K., Zhao, E., Sun, J.Z., Qin, A., Tang, B.Z., 2014. Sci. Rep. 4.
Yates, C.R., Benítez, D., Khan, S.I., Stoddart, J.F., 2007. Hexafunctionalized Borromeates using olefin cross metathesis. Org. Lett. 9, 2433–2436. https://doi.org/10.1021/ol070535y.
Zhang, W., Jin, Y. (Eds.), 2017. Dynamic Covalent Chemistry: Principles, Reactions, and Applications. John Wiley & Sons, Inc. https://doi.org/10.1002/9781119075738.